type compounds (*38*), or (iii) that the signal is from other plants that rarely synthesize oleanane precursors.

Finally, this data set introduces the quantitative use of the oleanane parameter in assessing angiosperm input to petroleum sources. Petroleum with measurable oleanane has almost certainly been generated from Cretaceous or younger source rocks, whereas that with an oleanane ratio >0.2 was probably derived from Tertiary sources.

## REFERENCES AND NOTES


1. H. L. ten Haven and J. Rullkötter, *Geochim. Cosmochim. Acta* **52**, 2543 (1988).
2. T. Bruun, *Acta Chem. Scand.* **8**, 1291 (1954).
3. H. Ageta and Y. Arai, *Phytochemistry* **22**, 1801 (1983).
4. ———, *Shoyakugaku Zasshi* **38**, 46 (Japanese, 1984).
5. M. C. Das and S. B. Mahato, *Phytochemistry* **22**, 1071 (1983).
6. E. V. Whitehead, in *Proceedings of Symposium on Hydrogeochemistry and Biogeochemistry*, Tokyo, Japan, 9 September 1970; E. Ingerson, Ed. (Clarke, Washington, DC, 1973), vol. II, pp. 158–211.
7. P. J. Grantham, J. Posthuma, A. Baak, in *Advances in Organic Geochemistry 1981*, M. Bjorøy *et al.*, Eds. (Wiley, Chichester, United Kingdom, 1983), pp. 675–683.
8. A. Riva, P. G. Caccialanza, F. Quagliaroli, *Org. Geochem.* **13**, 671 (1988).
9. M. R. Mello, P. C. Gaglianone, S. C. Brassell, J. R. Maxwell, *Mar. Petrol. Geol.* **5**, 205 (1988).
10. X. Zeng, S. Liu, S. Ma, in *Geochemical Biomarkers*, T. F. Yen and J. M. Moldowan, Eds. (Harwood Academic, Chur, Switzerland, 1988), pp. 25–49.
11. J. Fu and G. Sheng, *Appl. Geochem.* **4**, 13 (1989).
12. J. A. Doyle and L. J. Hickey, in *Origin and Early Evolution of Angiosperms*, C. B. Beck, Ed. (Columbia Univ. Press, New York, 1976), pp. 139–206.
13. N. F. Hughes, A. B. McDougall, J. L. Chapman, *J. Micropalaeontol.* **10**, 75 (1991).
14. J. A. Doyle and M. J. Donoghue, *Paleobiology* **19**, 141 (1993).
15. B. Cornet, *Mod. Geol.* **19**, 81 (1993).
16. K. H. Wolf, M. Gouy, Y. Yang, P. M. Sharp, W. Li, *Proc. Natl. Acad. Sci. U.S.A.* **86**, 6201 (1989).
17. W. Martin *et al.*, *Nature* **339**, 46 (1989).
18. W. Martin *et al.*, *Mol. Biol. Evol.* **10**, 140 (1993).
19. S. Lidgard and P. R. Crane, *Nature* **331**, 344 (1988).
20. P. R. Crane and S. Lidgard, *Science* **246**, 675 (1989).
21. L. J. Hickey and J. A. Doyle, *Bot. Rev.* **43**, 3 (1977).
22. D. W. Taylor and L. J. Hickey, *Syst. Evol.* **180**, 137 (1992).
23. K. J. Niklas, in *Patterns and Processes in the History of Life*, D. M. Raup and D. Jablonski, Eds. (Springer-Verlag, Berlin, 1986), pp. 383–405.
24. J. Muller, *Bot. Rev.* **47**, 1 (1981).
25. J. M. Moldowan, F. J. Fago, B. J. Huizinga, S. R. Jacobson, in *Organic Geochemistry. Advances and Applications in the Natural Environment*, D. A. C. Manning, Ed. (Manchester Univ. Press, Manchester, 1991), p. 195.
26. Major features of the mass spectra of 17α-hopane, lupane, 18α-oleanane, and 18β-oleanane (Fig. 1G) are remarkably similar, and various isomers or stereoisomers of hopane and lupane may coelute with the oleananes. With MRM GC-MS it was possible to take advantage of a small transition from the *m/z* 412 molecular ion ($M^+$) to the side-chain loss fragment *m/z* 369 that occurs in the spectra of 17α-hopane and lupane but is absent in the spectra of the oleananes. Other differences include a somewhat higher *m/z* 412→397 transition (loss of methyl) for the oleananes and the fact that oleananes typically occur as 18α and 18β isomers that can be partially resolved under the appropriate analytical conditions. The 18α to 18β isomer ratio can also be used as a maturity parameter (*8, 39*). MRM GC-MS analysis of a Wyoming shale (Fig. 1, A to C) detected an oleanane impostor, whereas analysis of a Trinidad shale (Fig. 1, D to F) detected low concentrations of oleananes.
27. Because immature shales in the Niger Delta were shown to have somewhat higher relative amounts of oleananes than mature ones (*40*), we used artificial maturation by pyrolysis to minimize the possible problems of comparing immature and mature samples. Analytical pyrolysis was carried out on crushed whole rock with commercial Rock-Eval instruments in which maximum generation ($T_{max}$) from the kerogen at temperatures <435°C is considered immature (*28*). Immature samples were crushed and pyrolyzed in evacuated sealed tubes at 300°C for 72 hours. Crushed rocks and pyrolyzed rocks were solvent extracted, and the extracts were fractionated by high-performance liquid chromatography (HPLC) as described (*28*). The HPLC-fractionated saturated hydrocarbons were analyzed for oleananes by MRM GC-MS (Fig. 1).
28. K. E. Peters and J. M. Moldowan, *The Biomarker Guide. Interpreting Molecular Fossils in Petroleum and Ancient Sediments* (Prentice-Hall, Englewood Cliffs, NJ, 1993).
29. M. Rohmer, P. Bisseret, S. Neunlist, in *Biological Markers in Sediments and Petroleum: A Tribute to Wolfgang K. Seifert*, J. M. Moldowan, P. Albrecht, R. P. Philip, Eds. (Prentice-Hall, Englewood Cliffs, NJ, 1992), p. 1.
30. G. Ourisson and P. Albrecht, *Acc. Chem. Res.* **25**, 398 (1992).
31. D. W. Taylor and L. J. Hickey, *Science* **247**, 702 (1990).
32. E. F. Wheeler, M. Lee, L. C. Mattern, *Bot. J. Linn. Soc.* **95**, 77 (1987).
33. S. L. Wing *et al.*, *Nature* **363**, 342 (1993).
34. Oleanane-triterpenoids and triterpenoid saponins are found throughout the angiosperms including monocot and dicot subclasses. They are most frequently found in members of the Dilleniidae, Rosidae, and Asteridae (*5, 41*). In the poorly sampled Magnoliidae (sensu Cronquist), these compounds are found throughout the herbaceous Ranunculales, although not in several woody magnolids (*42*). Further study of magnoliidean and gnetophyte phytochemistry is necessary to fully elucidate the distribution of oleanane-type compounds in living angiosperms. Finally, oleanane has been reported from the bennettitaleans, an extinct angiosperm sister group (*38*).
35. K. E. Peters *et al.*, *Am. Assoc. Pet. Geol. Bull.* **77**, 863 (1993).
36. A. E. Kontorovich *et al.*, *Sov. Geol. Geophys.* **32**, 1 (1991).
37. P. R. Crane, *Nature* **366**, 631 (1994).
38. D. W. Taylor, J. M. Moldowan, L. J. Hickey, 5th N. Amer. Paleontol. Conv. Abstr. Prog., *Paleontol. Soc. Spec. Pub.* **6**, 286 (1992).
39. C. M. Ekweozor and O. T. Udo, in *Advances in Organic Geochemistry 1987*, L. Matavelli and L. Novelli, Eds. (Pergamon, Terrytown, NY, 1988), pp. 131–140.
40. O. T. Udo and C. M. Ekweozor, *Energy Fuels* **4**, 248 (1990).
41. P. Pant and R. P. Rastogi, *Phytochemistry* **18**, 1095 (1979).
42. N. Basu and R. P. Rastogi, *ibid.* **6**, 1249 (1967).
43. J. M. Moldowan *et al.*, data not shown.
44. T. L. Phillips and W. A. DiMichele, in *Paleobotany, Paleoecology, and Evolution*, K. D. Niklas, Ed. (Praeger, New York, 1981), vol. 1, p. 231.
45. W. B. Harland *et al.*, *A Geologic Time Scale 1989*, (Cambridge Univ. Press, Cambridge, 1990).


46. We thank S. R. Jacobson for helpful discussions, C. Y. Lee and Q. Houh for sample preparations, M. M. Peña and P. Novotny for data acquisition, and Chevron Petroleum Technology Company for support of the work and permission to publish.

22 February 1994; accepted 31 May 1994


# The Temporal Distribution of Seismic Radiation During Deep Earthquake Rupture


Heidi Houston and John E. Vidale



**The time history of energy release during earthquakes illuminates the process of failure, which remains enigmatic for events deeper than about 100 kilometers. Stacks of teleseismic records from regional arrays for 122 intermediate (depths of 100 to 350 kilometers) and deep (depths of 350 to 700 kilometers) earthquakes show that the temporal pattern of short-period seismic radiation has a systematic variation with depth. On average, for intermediate depth events more radiation is released toward the beginning of the rupture than near the end, whereas for deep events radiation is released symmetrically over the duration of the event, with an abrupt beginning and end of rupture. These findings suggest a variation in the style of rupture related to decreasing fault heterogeneity with depth.**


The fundamental processes of earthquake initiation and termination are not well understood. The details of faulting are obscured by noise in seismograms, including the incoherence of the high-frequency wave field. In addition, it is difficult to simulate earthquake faulting adequately in the laboratory because of problems of scale, temperature, and pressure. Although the failure mechanism that generates deep seismicity remains unknown (*1*), it is likely that it and the rupture process change with depth in the Earth because ambient pressure and temperature increase with depth, $H_2O$ and $CO_2$ fluids are predicted to disappear below ~300 km (*2*), and phase changes may play a role in rupture at great depths (*3–7*). Furthermore, the source characteristics of earthquakes with depths greater than about 100 km are more easily studied


H. Houston, Institute of Tectonics, Earth Sciences Department, University of California, Santa Cruz, CA 95064, USA.
J. E. Vidale, United States Geological Survey, 345 Middlefield Road, Menlo Park, CA 94025, USA.

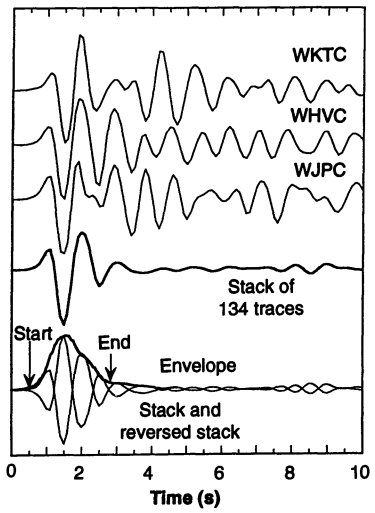


**Fig. 1.** Example of the stacked waveform and envelope for a typical earthquake. The top three traces are individual seismograms from the Northern California Seismic Array. Below them is shown the sum (or stack) of 134 records of this event. Summing together many records suppresses incoherent background noise generated near the receivers and reveals the termination of rupture. The envelope of the stack (bottom) is superimposed on the stack and the reverse of the stack to emphasize that an envelope is a smooth function that passes through the peaks of a time series.

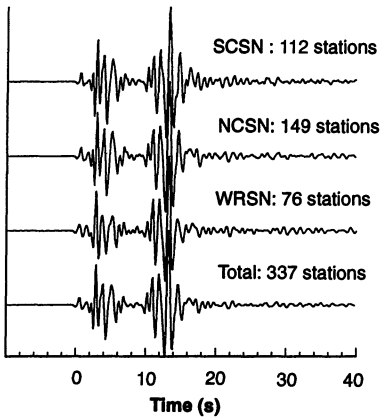


**Fig. 2.** Comparison of stacked waveforms from different arrays for one earthquake (23 June 1991). This event is unusually complex, but serves well to illustrate the consistency of the stacks at the different arrays; most events examined did not hesitate as this one did. SCSN indicates the Southern California Regional Network, NCSN the Northern California Seismic Network, and WRSN the Washington Regional Seismic Network. The event occurred at a depth of 570 km beneath Argentina with a moment of 8.6 × $10^{26}$ dyne-cm.

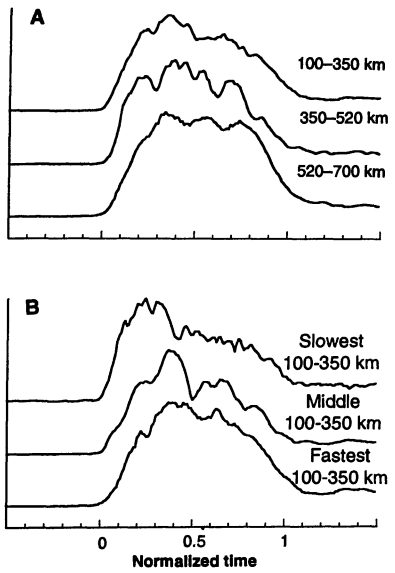


**Fig. 3.** Average envelopes of stacked waveforms. Before averaging, the envelope of each earthquake was stretched in time to equalize the duration, using durations measured from the stacks (*9*). Thus, for each stretched envelope, rupture begins at normalized time 0 and ends at normalized time 1 (*14*). (**A**) Average envelopes of stacks of events grouped by depth ranges 100 to 350, 350 to 520, and 520 to 700 km. The average envelope in the 100 to 350 km depth range is asymmetric, ending more slowly than it begins; at greater depths the average envelope is more symmetric. (**B**) Average envelopes of stacks of events in the 100 to 350 km depth range grouped by duration. The upper (middle, lower) envelope is the average of the 23 events with the longest (middle, shortest) scaled durations. The longer duration events have, on average, more asymmetric envelopes than do the shorter duration events.

than those of shallower events because seismic waves reflected from the Earth's surface arrive long enough after the direct body wave that this wave is not contaminated and, thus, can be more readily analyzed (*8*). Therefore, to explore changes in the failure mechanism with depth, we studied the rupture process of events deeper than 100 km. Specifically, we determined, in several depth ranges, the average temporal profile of short-period seismic radiation.

Although the initiation of faulting is generally easily identified on seismograms, later slip is often difficult to resolve. Summing together many short-period (0.5 to 5 s), teleseismic records from regional arrays enables the identification of rupture details and termination by canceling noise caused by incoherent reverberations near the stations (*9*) (Fig. 1). We summed together (or stacked) 30 to 200 vertical-component records of the P wave for each earthquake from one of three regional networks on the West Coast of the United States (*10*). The stacking process yields a similar stacked waveform (or stack) at each of the three arrays (Fig. 2) (*10*) The stack contains information from the source convolved with the instrument response.

We selected 122 events for analysis from 169 eligible earthquakes mainly on the basis of favorable radiation pattern and availability of data from at least one of the three arrays (*11*). The survey of earthquake durations by Vidale and Houston (*9*) revealed that, for a given earthquake size, durations are significantly shorter at greater depths, with a greater range of durations for events shallower than 350 km.

To determine the temporal pattern of the seismic radiation, we computed the envelope of each stack (Fig. 1). The envelope is always positive and essentially passes through the peaks of the stacks (*12*). It represents the temporal distribution of band-limited seismic radiation from the earthquake source (*13*). We then stretched each envelope in time to equalize the duration (*14*), using the durations picked from the stacks (*9*). Finally, we averaged the envelopes in three depth ranges.

For the deepest group of events, the average envelope (Fig. 3A) is quite symmetric in time, ending almost as abruptly as it begins (*15*). For events with depths between 350 and 520 km, the average envelope is somewhat more asymmetric in time, ending more gradually than it begins. For the shallowest group of events (those with depths between 100 and 350 km), the average envelope is even more asymmetric. Bearing in mind that the scaled durations decrease by about a factor of 2 as depth increases from 100 to 600 km (*9*), we infer that longer duration events have more asymmetric envelopes.

In consideration of the large variation in the scaled durations of events with depths between 100 and 350 km, we further grouped the events in this depth range into the fastest, middle, and slowest thirds, according to their durations, and averaged the values of the envelopes in these groups (Fig. 3B). Again, the events with long scaled durations have asymmetric envelopes, whereas the events with short scaled durations have much more symmetric envelopes. Evidently, even within the same depth interval, events with long scaled durations have a more gradual decrease in their short-period radiation.

Thus, in general, the temporal symmetry of the envelope is inversely related to the duration of the slip, which decreases significantly with depth (*16*). Evidently, intermediate depth events have longer scaled durations than deep events because the rupture of intermediate events tends to end more gradually. One of the possible explanations for the observed decrease in duration with depth given in (*9*) was that long duration events may simply have a slower rupture velocity as a proportion of shear-wave velocity, while being similar to shorter events in all other aspects of the rupture process such as stress drop or fault aspect ratio. Our result that the shape of

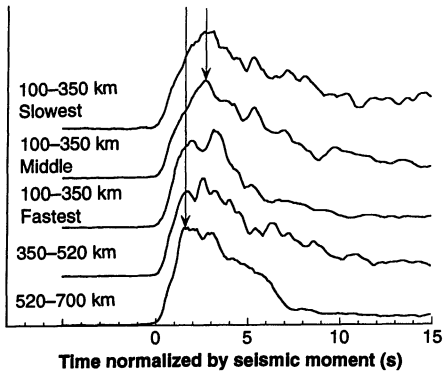


**Fig. 4.** Average envelopes of stacks of events in different depth ranges when time is scaled to the seismic moment of each earthquake rather than to the measured duration as in Fig. 3. Before averaging of the stacks, the time is scaled by the cube root of the seismic moment of the event (in units of $10^{26}$ dyne-cm). As in Fig. 3B, the envelopes labeled slowest, middle, and fastest represent the averages of the 23 events with the longest, middle, and shortest scaled durations. The slowest events in the 100 to 350 km depth range tend to start more slowly (see arrows) and end much more slowly than other events (note base line).

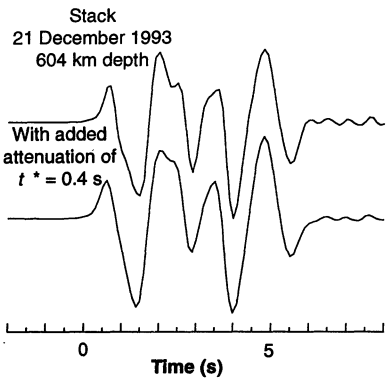


**Fig. 5.** Effect of attenuation on waveform. The stack (upper trace) of a large deep earthquake is convolved with an attenuation operator represented by a $t^*$ of 0.4 s to simulate the extra attenuation suffered by a 200-km-deep event compared to a 600-km-deep event. The result (lower trace) is similar to the original stack, which illustrates the minimal effect of the attenuation.

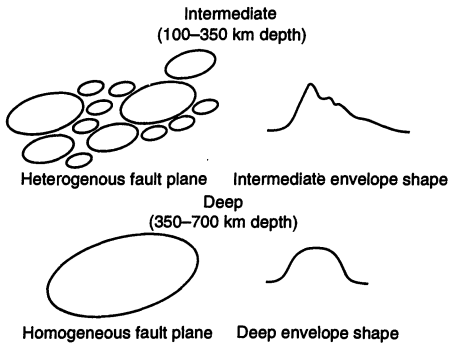


**Fig. 6.** Schematic illustration of the possible role of fault heterogeneity in envelope shape and rupture duration. Greater heterogeneity at intermediate depths may result in a relatively long duration and asymmetric envelope, whereas greater homogeneity deeper may result in a shorter duration and more symmetric envelope. The cartoon is intended to illustrate differences in the amplitude, as well as the scale length, of variations in physical properties in the subducting slab.

the envelope changes with depth rules this explanation out and favors the notion, developed below, that greater heterogeneity at intermediate depth leads to asymmetric envelopes.

Another scheme for scaling the envelopes before averaging them is to stretch the envelopes in time according to the cube root of their seismic moments (*17*) rather than the measured duration. Invariance under such a scaling is predicted by most earthquake source models (*18*). Scaling average envelopes according to the event moments emphasizes the change in duration with depth and shows that intermediate depth events tend to start somewhat slower and end much slower than deeper events (Fig. 4). Differences in the rise time of the envelopes can be interpreted more readily than with the previous procedure for scaling the envelopes before averaging (Fig. 3). On the other hand, the symmetry and termination of the rupture is difficult to evaluate in this scheme because of the averaging of events with a variety of durations, which was compensated for in the construction of Fig. 3. The envelope shapes in Fig. 4 are consistent with the observed decrease in rise times below about 450 km (*19*).

Seismic attenuation is concentrated in the upper 300 km of the mantle, so teleseismic waves from intermediate depth earthquakes undergo more attenuation than waves from deep earthquakes. We estimated the effect of the additional attenuation suffered by intermediate depth events by convolving an attenuation operator associated with a differential $t^*$ of 0.4 s with the stack of a deep earthquake (Fig. 5). The effect is small, and thus, the observed differences in envelope shape for deep and intermediate events (Figs. 3 and 4) cannot be attributed to attenuation.

The changes in rupture style with depth found here may be associated with increasing homogeneity in material properties as lithosphere descends through the upper mantle (Fig. 6). Deeper subducted lithosphere is subject to greater temperature, pressure, and time at depth, which tend to promote greater homogeneity in material properties. Both the slab thermal structure (*20*) and mineralogy (*21*), for example, are likely more homogeneous at depths of 500 to 600 km than of 200 to 300 km. Temporally asymmetric faulting of longer duration could be related to greater heterogeneity at intermediate depth, which could enhance heterogeneity in the distribution of slip during a single earthquake (*22*). The duration and asymmetry would be controlled by the tendency of the largest moment-releasing subevent to produce the most immediate aftershocks or to distribute stress onto the lower slip regions surrounding it, breaking them and prolonging rupture with a small amount of slip.

Another reason that faults deeper than 400 km could be more homogeneous is related to the hypothesis that deep earthquakes are caused by a shear instability associated with the transformation of metastable olivine to its high-pressure phases within the cold core of subducting slabs (*3–5*). This hypothesis implies that faulting below 400 km in depth occurs only on new faults, which would likely be more homogeneous structures than reactivated faults (*23*). In contrast, intermediate-depth earthquakes are thought to occur through fluid-assisted cracking (the Terzagi effect) (*3–5, 7*), in which case fault reactivation may play a role. Although partial transformation associated with the transformational faulting of metastable olivine could lead to greater heterogeneity in the deep slab (*24*), only untransformed regions, presumably more homogeneous, are expected to undergo the shearing instability. (That is, the heterogeneity relevant to this process is that on a given fault plane before the shearing instability occurs, rather than in the surrounding regions.)

This and other recent studies have found changes in several aspects of fault rupture processes with depth, including the shape of the envelope of seismic radiation presented here, earthquake durations (*9*), rise times (*19*), and aftershock production (*24*). Variations in rupture processes with depth have been difficult to discern previously, although they may be expected on the basis of known changes in material properties from the Earth's surface through the transition zone. These variations should help constrain the physical mechanism by which deep earthquakes occur, which remains unknown.

Furthermore, if the association between envelope shape and rupture duration for earthquakes deeper than 100 km holds for events at shallower depths as well, then shallow faulting may be strongly controlled by fault heterogeneity. An understanding of this association would have important implications for seismic hazard.

## REFERENCES AND NOTES

1. Although brittle frictional failure is believed to generate earthquakes on shallow faults, frictional processes such as fracture or sliding on a preexisting fault surface become inhibited as depth and, consequently, pressure increase; further-

more, high temperatures at depth promote ductile flow, rather than fracture, to relieve stress [H. Jeffreys, *The Earth, Its Origin, History and Physical Constitution* (Cambridge Univ. Press, Cambridge, ed. 2, 1929); H. Jeffreys, *Proc. R. Soc. Edinburgh* **56**, 158 (1936); M. S. Paterson, *Experimental Rock Deformation: the Brittle Field* (Springer-Verlag, New York, 1978)].
2. A. B. Thompson, *Nature* **358**, 295 (1992); S. Kraft, E. Knittle, Q. Williams, *J. Geophys. Res.* **96**, 17997 (1991).
3. H. W. Green and P. C. Burnley, *Nature* **341**, 733 (1989).
4. P. C. Burnley, H. W. Green, D. J. Prior, *J. Geophys. Res.* **96**, 425 (1991); H. W. Green, T. E. Young, D. Walker, C. Scholz, *Nature* **348**, 720 (1990).
5. S. H. Kirby, W. B. Durham, L. A. Stern, *Science* **252**, 216 (1991).
6. D. C. Rubie and C. R. Ross, *Eos* **73**, 378 (1992).
7. C. Meade and R. Jeanloz, *Science* **252**, 68 (1991).
8. To perform a global study of the detailed rupture process of large earthquakes, teleseismic records of body waves generally have proved the most useful, as well as the most abundant, data set. Recent work with near-field, broad-band body waves to study the source, such as those recorded by TERRAscope in southern California, would not be possible on a global scale because of the lack of dense coverage by broad-band seismometers.
9. J. E. Vidale and H. Houston, *Nature* **365**, 45 (1993).
10. We used records from the Southern California Seismic Network, the Northern California Seismic Network, or the Washington Regional Seismic Network, depending on the availability of data. The similarity of the waveform produced by stacking records at each of the three arrays for a particular event justifies using the arrays interchangeably according to which array recorded and archived a given event.
11. During the period from April 1980 to June 1992, 169 earthquakes occurred between 35° and 90° from California, with seismic moments greater than $1.6 \times 10^{25}$ dyne-cm and depths greater than 100 km. Events with nodal P-wave radiation coefficients (<0.1) were excluded, as were a few events for which the end of rupture could not be reliably inferred or for which the rupture appeared to stop and then restart. The remaining 122 events were used in (*9*) and in the analysis presented here.
12. The envelope of a time series is given by the square root of the sum of the squares of the time series and its Hilbert transform [E. R. Kanasewich, *Time Sequence Analysis in Geophysics* (Univ. of Alberta Press, Alberta, Canada, 1981)].
13. The frequency content of our stacks is controlled by the response of the instruments used in the short-period regional arrays, which is peaked between 0.5 and 4 Hz, and the source spectrum, which is peaked in velocity around the corner frequency (which varies from 0.2 to 2 Hz for these earthquakes). Hence, we obtain envelopes of band-limited seismic radiation. The envelope is similar in shape to the source time function if the shape of the source spectrum does not change during the rupture. Only for band-limited radiation can we get a noise-free and detailed picture of the time-dependent rupture.
14. In this scheme, each envelope is stretched in time so that rupture begins at normalized time 0 and ends at normalized time 1. Use of this scheme to stretch the envelopes before averaging equalizes the durations of the envelopes, removing the effects of earthquake size and duration and preserving only the shape. Thus, the resulting average envelope shape is not affected by changes in fault parameters that affect the duration in a simple way, such as rupture velocity or stress drop under a constant spectral source model. Furthermore, this scheme has the advantage that the first-order effects of directivity (those due to unilateral rupture), which could affect the duration of the stack (and, hence, the duration of the envelope), do not affect the envelope shape. Hence, the use of this scheme ensures that the resulting average envelope shape could not be affected much by systematic differences in directivity, if they are present.
15. The shape of the average envelope for the deepest group of earthquakes is consistent with the common practice in source modeling of parameterizing the time function as the convolution of two boxcars (one representing the duration of rupture over the entire fault and the other the duration of slip at a particular point on the fault).
16. Vidale and Houston (*9*) measured durations of 122 deep and intermediate earthquakes from stacks and found a decrease in the duration (when corrected for earthquake moment) of about a factor of 2 from 100 to 600 km depth. If the parameters that describe rupture (which include stress drop, fault geometry, the ratio of rupture velocity to shear velocity, and the intermittency of slip) have no systematic trend with depth, durations should decrease with depth at the same rate that the shear velocity increases with depth, according to a simple scaling model. But shear velocity increases only about 20% between 100 and 600 km in depth. Thus, the observation that durations decrease by a factor of 2 requires that one or more of the rupture parameters change significantly with depth. However, a simple increase in stress drop with depth, which would decrease the duration, would not be sufficient to change the envelope shape from asymmetric to symmetric (Fig. 3A). Furthermore, work by Houston and Williams (*19*) indicates that average stress drops do not change significantly between 100 and 600 km in depth. Nor would an increase with depth in rupture velocity as a proportion of shear velocity, which could explain the decrease in duration with depth, produce the difference in envelope shapes.
17. Seismic moments are taken from the Harvard Centroid Moment Tensor catalog [A. M. Dziewonski and J. H. Woodhouse, *J. Geophys. Res.* **88**, 3247 (1983)].
18. H. Kanamori and D. L. Anderson, *Bull. Seismol. Soc. Am.* **65**, 1073 (1975).
19. H. Houston and Q. Williams, *Nature* **352**, 520 (1991).
20. D. L. Turcotte and G. Schubert, *Geodynamics* (Wiley, New York, 1982).
21. T. Irifune and A. E. Ringwood, *High-Pressure Research in Mineral Physics*, M. H. Manghnani and Y. Syono, Eds. (American Geophysical Union, Washington, DC, 1987), pp. 231–242; C. B. Agee, *Annu. Rev. Earth Planet. Sci.* **21**, 19 (1993).
22. The lengths relevant to our seismic observations are on the scale of kilometers rather than meters. Thus, variations in properties over kilometers is probably more pertinent than, for example, absolute grain size.
23. Green and Burnley (*3*), for example, found that, in experiments on germanate olivine under deviatoric stress, spinel-filled anti-cracks (analogous to Mode I cracks in brittle failure [C. Scholz, *The Mechanics of Earthquakes and Faulting* (Cambridge Univ. Press, Cambridge, 1990), chap. 1] appear to link up into throughgoing Mode II and III structures, on which shear slip occurs. This process occurs through the growth and self-organization of the Mode I anti-cracks at the tip of a growing fault and is believed to occur only once on a given planar structure (H. Green, personal communication). The spinel contents of the anti-cracks are spilled into the growing fault zone, giving it a super-plastic rheology. However, after faulting stops the spinel coarsens to a grain size that is no longer super-plastic, and the fault is, therefore, not able to slip again.
24. The incidence of aftershocks is considerably less common for events deeper than 80 km than for shallower events. Below 450 km there is a moderate increase in the incidence of aftershocks compared to events at depths of 80 to 450 km [C. Frohlich, *J. Geophys. Res.* **92**, 13944 (1987)].
25. We thank J. Savage, W. Thatcher, and Q. Williams for comments on the manuscript and D. Farber and H. Green for helpful suggestions. Supported partially by the National Science Foundation and the W. M. Keck Foundation.

3 January 1994; accepted 2 June 1994

# Orientation Selectivity of Cortical Neurons During Intracellular Blockade of Inhibition

Sacha Nelson,* Louis Toth, Bhavin Sheth, Mriganka Sur

**Neurons in the primary visual cortex of the cat are selectively activated by stimuli with particular orientations. This selectivity can be disrupted by the application of antagonists of the inhibitory neurotransmitter γ-aminobutyric acid (GABA) to a local region of the cortex. In order to determine whether inhibitory inputs are necessary for a single cortical neuron to show orientation selectivity, GABA receptors were blocked intracellularly during whole cell recording. Although the membrane potential, spontaneous activity, subfield antagonism, and directional selectivity of neurons were altered after they were perfused internally with the blocking solution, 18 out of 18 neurons remained selective for stimulus orientation. These results indicate that excitatory inputs are sufficient to generate orientation selectivity.**

The ability to respond selectively to contours of a particular orientation is a common feature of visual cortical neurons and is believed to underlie the first stages of the perception of form. Attempts to understand the cellular mechanism of orientation selectivity have led to conflicting interpretations. Intracellular recording studies (*1–4*) have generally supported the hypothesis that orientation selectivity arises from the pattern of convergence of excitatory afferents from the lateral geniculate nucleus (LGN) (*5*). Other studies, especially those that employ local application of bicuculline, a blocker of receptors for $GABA_A$, have demonstrated the importance of inhibition in maintaining selectivity (*6, 7*). An

Department of Brain and Cognitive Sciences, Massachusetts Institute of Technology, Cambridge, MA 02139, USA.

*To whom correspondence should be addressed.